Advanced Ceramics Progress: Vol. 11, No. 3, (Summer 2025) 13-23

Materials and Energy Research Center
MERC

Contents lists available at ACERP

Advanced Ceramics Progress

Journal Homepage: www.acerp.ir

Original Research Article

Ca-Al Layered Double Hydroxide/ZIF-67 Metal-Organic Framework (LDH/MOF) Nanocomposites for Drug Delivery Application

Arezoo Mohajer Heravi [a], Mohammad Jafar Molaei [b]*, Jafar Abdi [b, c]

[a] *MS Student, Faculty of Chemical and Materials Engineering, Shahrood University of Technology, P. O. Box: 3619995161, Shahrood, Iran.*
[b] *Associate Professor, Faculty of Chemical and Materials Engineering, Shahrood University of Technology, P. O. Box: 3619995161, Shahrood, Iran.*
[c] *Associate Professor , Department of Chemical Engineering, Faculty of Engineering, University of Zanjan, P. O. Box: 451561319, Zanjan, Iran.*
* Corresponding Author Email: m.molaei@shahroodut.ac.ir (M. J. Molaei) URL: https://www.acerp.ir/article_243774.html

ARTICLE INFO

Article History:
Received 18 October 2025
Received in revised form 16 November 2025
Accepted 17 February 2026

Keywords:
Ca-Al Layered Double Hydroxide,
ZIF-67 Metal-Organic Framework (MOF),
Drug Delivery,
pH-Dependent Drug Release

ABSTRACT

Layered double hydroxides (LDHs) are 2D layered materials with a high specific surface area. Metal-organic frameworks (MOFs) are porous structures with adjustable pore size and surface area. In this research, the Ca-Al LDH/ZIF-67 MOF (LDH/MOF) nanocomposite was synthesized through coprecipitation and evaluated for its application as a nanocarrier in drug delivery systems. FESEM images showed that LDH nanosheets are decorated with ZIF-67 particles, and they can also enter the spacing between the LDH layers. The synthesized LDH/MOF nanocomposite exhibited a significantly enhanced surface area of 60.8 m^2/g with an average pore diameter of 2.1 nm, compared to LDH (6.53 m^2/g, 6.6 nm) and MOF (11.2 m^2/g, 4.9 nm) samples. The synthesized LDH/MOF nanocomposite was investigated for drug release behavior using ciprofloxacin as the model drug. The nanocomposite showed a drug loading efficiency and drug loading capacity of 58% and 19%, respectively. The LDH/MOF nanocomposite exhibited pH-dependent drug release, reaching 64% and 85% within 12 h at pH 7.4 and 5.3, respectively. The drug release from the LDH/MOF nanocomposite follows the Korsmeyer-Peppas model and is estimated to occur through quasi-Fickian diffusion. The Ca-Al LDH/MOF nanocomposite is promising for application in drug delivery systems, with enhanced release in acidic tumor microenvironments.

https://doi.org/10.30501/acp.2026.554046.1186

1. INTRODUCTION

Due to the transformation cycle, long development time, and high cost associated with developing novel drugs, it is more efficient to use traditional drugs more effectively. Therefore, the concept of drug delivery systems was introduced in 1960. Drug delivery systems have the potential to protect drugs from degradation in vivo, solubilize hydrophobic drugs, transport them to specific sites in the body, and release them at a controlled rate (Kuang et al., 2021). Several kinds of nanovehicles such as inorganic nanoparticles (Yanar et al., 2023), polymers (Sung & Kim, 2020), hydrogels (Thang et al., 2023), dendrimers (Nikzamir et al., 2021), liposomes (Guimarães et al., 2021), quantum dots (Molaei, 2022; Molaei & Salimi, 2022), carbon nanotubes (Abdallah et al., 2020), and metal–organic framework (Lawson et al., 2021) nanocarriers have been used for the controlled release of drugs and bioactive molecules. Several factors such as biodegradability, biocompatibility, storage, and facile synthesis are the main factors for an ideal drug delivery nanovehicle (Kumari et al., 2023). Different nanoparticles such as gold nanoparticles (Cosma et al.,

Please cite this article as: Mohajer Heravi, A., Molaei, M. J. & Abdi, J. (2025). Ca-Al Layered Double Hydroxide/ZIF-67 Metal-Organic Framework (LDH/MOF) Nanocomposites for Drug Delivery Application, *Advanced Ceramics Progress*, 11(3), 13-23. https://doi.org/10.30501/acp.2026.554046.1186

2025), silica nanoparticles (Ilyes et al., 2025), graphene (Roondhe et al., 2025), carbon nanotubes (Das et al., 2025), MOFs (Kazemi et al., 2025), and LDHs (Molaei, 2023a) have been used in drug-delivery systems for the treatment of cancer. Nanoparticles with reduced side effects and enhanced effectiveness can deliver chemotherapy drugs directly to cancer cells (Elumalai et al., 2024).

Two-dimensional nanostructures such as graphene (Wekalao et al., 2025), metal carbides and nitrides (MXenes) (Mahapatra et al., 2025), hexagonal boron nitride (h-BN) (Ramezanzadeh et al., 2025), bismuth-based layered compounds (Barot et al., 2025), transition metal dichalcogenides (TMDs) (Patra et al., 2025), and layered double hydroxides (LDHs) (Wu et al., 2025) have received research interests during recent years. 2D materials possess narrow thickness and double-sided surface structure with enhanced specific surface area and increased exposed active sites. Among them, LDHs can be considered an emerging class of 2D nanostructures in natural or synthetic anionic clay minerals categories. These synthetic structures have the general formula of $[M^{2+}_{1-x}M^{3+}_{x}(OH)_2(A^{n-})_{x/n}]^{x+}$ .mH_2O in which M^{2+} is metallic ion such as Cu^{2+}, Zn^{2+}, Co^{2+}, Ni^{2+}, Mg^{2+}, etc. and M^{3+} is also metal ion such as Cr^{3+}, Al^{3+}, V^{3+}, Fe^{3+}, Ga^{3+}, etc. $A^{n-}$is an anion such as CO_3^{2-}, NO_3^-, Cl^-, and SO_4^{2-}. X is $M^{3+}/M^{2+}+M^{3+}$ratio which lies in the range of 0.2-0.33 for pure LDH phase. The anions which are intercalated between metal ions-containing layers will balance the extra positive charge of these layers (Karim et al., 2022).

LDHs can be synthesized through hydrolysis, sol-gel, hydrothermal, and co-precipitation methods, among which co-precipitation is the most conventional approach for synthesizing LDH nanosheets. The co-precipitation synthesis of LDHs involves mixing metal salts at a certain molar ratio, followed by the addition of an alkali solution and an aging step after precipitation (Molaei, 2023b). The interlayer spacing, which is the distance between the two host layers, is influenced by the type of cations and anions. LDHs exhibit a variety of types and structures due to variables such as interlayer spacing and composition. However, hexagonal nanosheets are the dominant morphology of LDHs (Jing et al., 2020).

Drug molecules can be intercalated into the layered channels of the LDH structure instead of the interlayer anions, which results in improved drug loading efficiency (Chen et al., 2017). The increasing interest in LDHs as vehicles in drug delivery systems is attributed to their properties such as large storage capacity, biodegradability, biocompatibility, and capability for modified drug release.

The suitable performance of LDHs in biological environments is related to their surface properties, layer charge density, particle size, and chemical composition. Therefore, modifications in synthesis parameters can regulate the release rate of the loaded drug (Figueiredo et al., 2018). Combining LDHs with other nanostructures such as nanoparticles, anions, surfactants, and polymers can further improve the surface characteristics of the resulting nanomaterials (Daud et al., 2019).

Metal-organic frameworks (MOFs), coordination polymers, and zeolites are examples of porous materials that have received major attention in recent years. These materials are classified as porous solids because they contain highly organized micro- and mesoporous structures capable of accommodating and transporting guest species. Their high pore volume and tunable pore environments are crucial for applications such as adsorption, gas storage, catalysis, and controlled drug delivery, where efficient diffusion pathways and large accessible surface areas directly influence performance (Adegoke & Maxakato, 2021; Behera et al., 2021; Derbe et al., 2021; Kitagawa & Matsuda, 2007; Möller & Bein, 2013). MOFs with high porosity, often containing up to 90% free volume, also possess large surface areas (Deeraj et al., 2023). MOFs are crystalline porous solid structures with adjustable and accessible pores, wide surface area, straightforward synthesis procedures, the possibility for incorporation of active species or functional groups without altering the topology, and the availability of coordination-unsaturated sites (Li et al., 2023).

MOFs consist of inorganic metal ion clusters and organic ligands connected by moderately strong coordination bonds (Fattah-alhosseini et al., 2023). When metal ions, acting as nodes, are bridged by organic linkers, a cage-like configuration with high porosity is formed. Variations in linkers and metal nodes result in changes in properties such as specific surface area, density, and pore size (Roslan & Aris, 2023). MOFs have been applied in biological imaging and sensing, fuel cells, water treatment, gas separation and storage, and drug delivery (Fattah-alhosseini et al., 2023). Their use in drug delivery systems has been widely investigated in recent years. A broad range of drugs, including nucleic acids, proteins, and small molecules, can be loaded into MOFs. Controlled drug release can be achieved by modifying the chemical functionality and pore size of MOFs (Rabiee, 2023).

Among MOFs, the zeolite imidazolate framework (ZIF) is noteworthy due to properties such as thermal stability and large surface area (Qing et al., 2023). ZIFs are composed of transition metals such as Co and Zn bridged by N atoms from imidazolate or functionalized imidazolate units. ZIFs possess the advantageous characteristics of both MOFs and zeolites. They exhibit excellent structural tunability based on channels and cages within the framework. They also show chemical and mechanical stability due to robust metal–nitrogen bonds compared to other MOFs (Jin & Shang, 2021). ZIF-67 is a cobalt-based ZIF MOF in which cobalt ions are interconnected with 2-methyl imidazole linkers, with

four nitrogen atoms from four 2-methyl imidazole ligands coordinating each cobalt ion. In ZIF-67, two cobalt centers are bridged by a 2-methyl imidazole ligand. ZIF-67 can be synthesized through a one-step co-precipitation reaction (Mohamed et al., 2021).

Previous studies have developed various LDH/MOF-based nanocomposites for drug delivery, such as ZIF-67@Co-LDH yolk–shell structures (Chen et al., 2019), ZIF-8@LDHs core–shell systems (Wang et al., 2023), and Alg-DOX-Cu MOF-LDH beads (Karimi et al., 2023). Although these systems demonstrated improved drug loading and controlled release, many lacked strong pH responsiveness or exhibited limited stability and targeting in acidic tumor environments. Furthermore, the MgAl-LDH/Fe-MOF/D-Man system (Pooresmaeil & Namazi, 2022), despite its success in co-delivery and bioimaging, required a complex multi-step synthesis process that reduced scalability and reproducibility.

Considering these limitations, there remains a need for a simpler LDH/MOF nanocomposite with higher surface area, efficient drug loading, and controlled pH-responsive release suitable for tumor microenvironments. The current study addresses these gaps by focusing on a Ca-Al LDH/MOF nanocomposite designed to combine the structural advantages of both LDH and MOF frameworks for enhanced drug delivery performance. The unique properties of LDH, including its intercalation capability and biocompatibility, make it a suitable matrix for drug delivery when combined with MOF. The Ca–Al LDH system was selected instead of the more commonly used Mg–Al or Zn–Al LDHs because Ca is a biologically essential and highly biocompatible cation. In addition, Ca–Al LDHs typically possess larger interlayer spacing due to the ionic radius of Ca^{2+}, which facilitates higher drug loading and more efficient intercalation of bulky drug molecules. The resultant nanocomposite can therefore benefit from the LDH structure with interlamellar spacing for drug loading, and from the MOF framework as a porous structure with high surface area. Ciprofloxacin was used as the model drug to investigate the loading and release properties of the LDH/MOF nanocomposite.

2. MATERIALS AND METHODS

2.1. Materials

Calcium nitrate ($Ca(NO_3)_2{\cdot}4H_2O$), aluminum nitrate ($Al(NO_3)_3{\cdot}9H_2O$), sodium carbonate (Na_2CO_3), sodium hydroxide (NaOH), sodium dodecyl sulfate (SDS) with the chemical formula ($CH_3(CH_2)_{11}OSO_3Na$), urea (NH_2CONH_2), 2-methylimidazole ($CH_3C_3H_2N_2H$), cobalt nitrate ($Co(NO_3)_2{\cdot}6H_2O$), and methanol (CH_3OH) were obtained from Merck. Ciprofloxacin was purchased from Shahid Ghazi Pharmaceutical Co. All chemicals were of analytical grade and used without further purification.

2.2. Synthesis of Ca-Al LDH

Ca-Al LDH nanosheets were synthesized according to the previous work in ref. (Shahabadi et al. 2019). Briefly, 3.4 g of calcium nitrate and 1.8 g of aluminum nitrate were added to 60 ml of a deionized water and methanol mixture (V_deionized water:V_methanol = 1:1). Then, 0.17 g of urea and 0.017 g of sodium dodecyl sulfate were added to the solution and stirred until completely dissolved, yielding a transparent solution (solution A).

Solution B was prepared by adding 0.96 g of sodium hydroxide and 0.64 g of sodium carbonate to 20 ml of deionized water, stirring until fully dissolved, followed by adjusting the total volume to 100 ml with deionized water. Solution B was then added dropwise to solution A until the pH reached 10. The suspension was treated with a 750 W ultrasonic probe for 5 min to facilitate delamination of the LDH layers. The suspension was then stirred for 6 h and aged for 24 h. Subsequently, the precipitates were collected using a 4000 rpm centrifuge, washed several times to reach neutral pH, and dried at 80 °C overnight.

2.3. Synthesis of LDH/MOF Nanocomposites

Synthesis of the MOF was performed through co-precipitation in the presence of LDH nanosheets. Briefly, 0.07 g of LDH nanosheets and 0.11 g of cobalt nitrate were added to 30 ml of deionized water and stirred for 10 min, followed by 5 min of ultrasonication using a 750 W ultrasonic probe.

Another solution was prepared by dissolving 1 g of 2-methylimidazole in 20 ml of deionized water, which was added dropwise to the LDH-containing suspension under vigorous stirring. The suspension turned purple due to the formation of MOFs.

Stirring was continued for an additional 2 h, and the suspension was then aged for 24 h at room temperature. The precipitates were collected by centrifugation and washed several times with deionized water to reach a neutral pH. The formed LDH/MOF particles were dried at 80 °C overnight and then ground in an agate mortar for subsequent experiments.

2.4. Drug Loading

For drug loading experiments, ciprofloxacin was used as the model drug. A total of 0.016 g of the LDH/MOF sample was added to 2 ml of ciprofloxacin solution with a concentration of 20 mg ml^{-1}. The ciprofloxacin solution was sonicated for 10 min to ensure complete dissolution and homogeneity before mixing with the nanocomposite, and the pH was maintained at 7.4 during the loading process. The suspension was stirred vigorously for 8 h in the dark, and the particles were collected using a 4000 rpm centrifuge and dried at 70 °C overnight. The remaining drug content in the supernatant was measured by UV–visible absorption at 322 nm. The drug loading efficiency and drug loading capacity were calculated using the following formula (Molaei, 2023a):

$$\text{Loading efficiency} = \frac{\text{Mass of the drug loaded on the particles}}{\text{total amount of drug}} \times 100 \quad (1)$$

$$\text{Drug loading capacity (\%)} = \frac{\text{Amount of loaded drug on the particles}}{\text{mass of the drug-loaded carrier}} \times 100 \quad (2)$$

2.5. Drug Release

Drug-release experiments were performed by dispersing 0.102 g of drug-loaded particles in 5 ml of PBS inside a 12 kDa-cutoff dialysis tube, which was then immersed in 30 ml of PBS under gentle shaking. The experiments were conducted at 37 °C to simulate physiological conditions. At predetermined time points, 5 ml of the external PBS was withdrawn and replaced with an equal volume of fresh PBS to maintain equilibrium in the system. The drug content in the collected samples was quantified using UV–visible spectroscopy. Drug concentrations were determined from a calibration curve. To generate the calibration curve, the UV–visible absorbance of PBS solutions containing known drug concentrations was recorded, and the absorbance at 322 nm was used for plotting the curve. The percentage of drug released was calculated using the following formula:

$$\text{Drug release (\%)} = \frac{\text{The amount of released drug}}{\text{the amount of loaded drug on the particles}} \times 100 \quad (3)$$

Figure 1 represents a schematic that shows the synthesis method, drug loading, and release procedure of the LDH/MOF nanocomposite.

2.6. Characterization

Phase analysis was performed using a D8-Advance Bruker diffractometer with Cu-Kα radiation and a step size of 0.05° over the 2θ range of 5–75°. The chemical bonding and functional groups of the samples were examined by Fourier transform infrared spectroscopy (FTIR) (Beijing Rayleigh WQF-510). The concentration of the drug in the samples was determined by UV–visible spectroscopy (Rayleigh-2601), based on a calibration curve derived from samples with different drug dilutions. The surface area of the samples was measured using a Quantachrome Autosorb-1-MP BET analyzer. The size and morphology of the samples were characterized using a ZEISS Sigma 300 FESEM.

3. RESULTS AND DISCUSSION

Figure 2a shows the XRD patterns of Ca–Al LDH nanosheets, MOF, and the LDH/MOF nanocomposite. It can be seen that the Ca–Al LDH XRD pattern contains the main characteristic LDH peaks. These peaks are consistent with the XRD data of LDHs reported in the literature (Bai et al., 2025). The conformation of the intercalated anions within the interlayer spacing of the LDH nanosheets can be inferred from the d-spacing, which can be deduced from the broadening of the XRD peaks. Theoretically, the long axis of the MO molecule has a dimension of 1.31 nm. Considering a thickness of 0.48 nm for one monolayer of LDH, a basal spacing of 1.79 nm can be calculated for a monolayer oriented perpendicular to the interlayer spacing (Zhang et al., 2012). The interplanar spacing for the synthesized LDH nanosheets is 4.42 nm, based on the XRD peak broadening calculated using the Scherrer equation. The interlayer spacing of SDS-intercalated LDH is larger than that of organic LDH (Chen et al., 2016). The XRD pattern of the MOF sample matches that of ZIF-67. As shown in Figure 2, distinct 2θ diffraction peaks appear at 7.8°, 11.6°, 15.2°, 17.9°, 19.1°, 21.8°, and 25.1°, corresponding to the (011), (112), (022), (013), (114), (223), and (224) crystal planes. These peaks align with the typical crystalline pattern of ZIF-67, consistent with previous reports (Diop et al., 2025). The XRD pattern of the LDH/MOF nanocomposite indicates that LDH has preserved its structure, and MOF particles have formed within the nanocomposite.

The zeta potential distribution curve of the synthesized LDH/MOF nanocomposite is shown in Figure 2b. The zeta potential of the sample is 3.4 mV, which is not sufficiently large to exert effective steric repulsion between particles. Figure 2c shows the FTIR spectra of LDH, MOF, and the LDH/MOF nanocomposite. The vibration bands around 1435 and 1469 cm^{-1} in the FTIR spectrum of LDH are attributed to the stretching of carboxylate groups. The typical M–O vibration appears at 521 cm^{-1} (Plank et al., 2006). The peak at 875 cm^{-1} indicates the presence of nitrate. The absorption band at 1625 cm^{-1} can be assigned to the H–O–H bending vibration (Jadam et al., 2021). The peak at 1407 cm^{-1} corresponds to the stretching vibration of interlayer CO_3^{2-} (Sun et al., 2017). The peak at 1801 cm^{-1} corresponds to the asymmetric and symmetric vibrations of the COO^- stretch. The peak at 3471 cm^{-1} is related to the adsorption of water molecules on the surface and the hydroxyl groups (Kuang et al., 2021). The peak at 2923 cm^{-1} is due to the O–H stretching vibration. The peak at 3455 cm^{-1} can also be attributed to the stretching and bending vibration of O–H groups (Wang et al., 2022). For the ZIF-67 FTIR spectrum, the characteristic bending and stretching vibrational modes of the imidazole ring can be observed at 752 cm^{-1}, 991 cm^{-1}, 1141 cm^{-1}, 1303 cm^{-1}, 1419 cm^{-1}, 1569 cm^{-1}, 2919 cm^{-1}, and 3131 cm^{-1} (Jiang et al., 2023). The FTIR spectrum of the LDH/MOF nanocomposite displays the characteristic peaks of both phases. However, the strong peak of LDH at 1434 cm^{-1} has shifted to 1415 cm^{-1}, which may be attributed to interactions occurring between the two phases. Figure 3a shows the FESEM image of the synthesized LDH nanosheets. The LDH platelets exhibit a crystalline morphology and are well-delaminated. The FESEM image of the MOF particles in Figure 3b shows monodispersed particles with a polygonal morphology, indicating successful synthesis of the MOF phase.

The FESEM image of the LDH/MOF nanocomposite in Figure 3c shows that the LDH nanosheets are decorated with MOF particles exhibiting their polygonal morphology. Furthermore, some MOF particles appear to have penetrated the interplanar spacing of the LDH nanosheets. The EDS mapping of the LDH/MOF nanocomposite confirms the uniform distribution of both phases (Figure 1S).

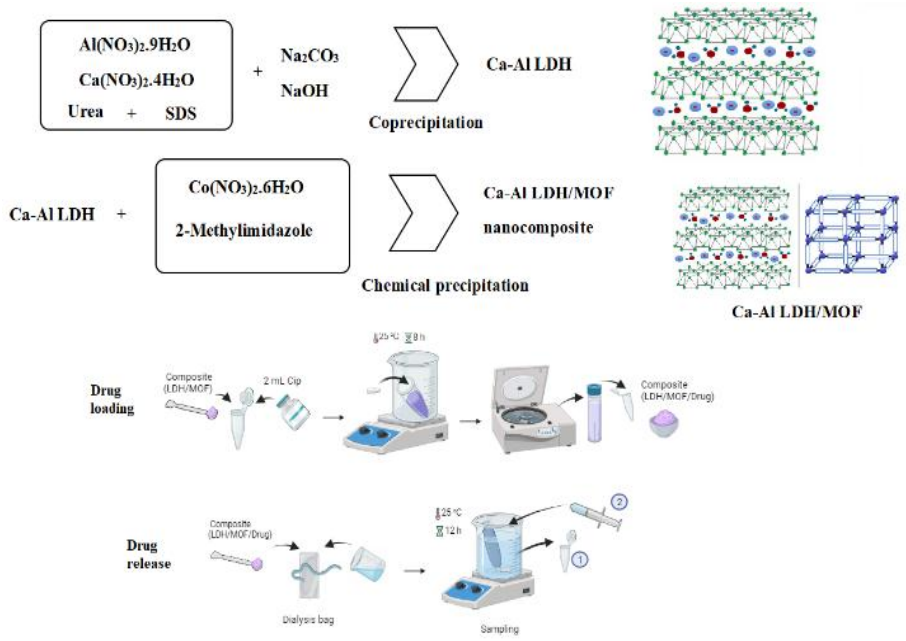

Figure 1. Schematic that shows the synthesis method, drug loading, and release procedure of the LDH/MOF nanocomposite (Aftab et al., 2025; Umdor et al., 2025).

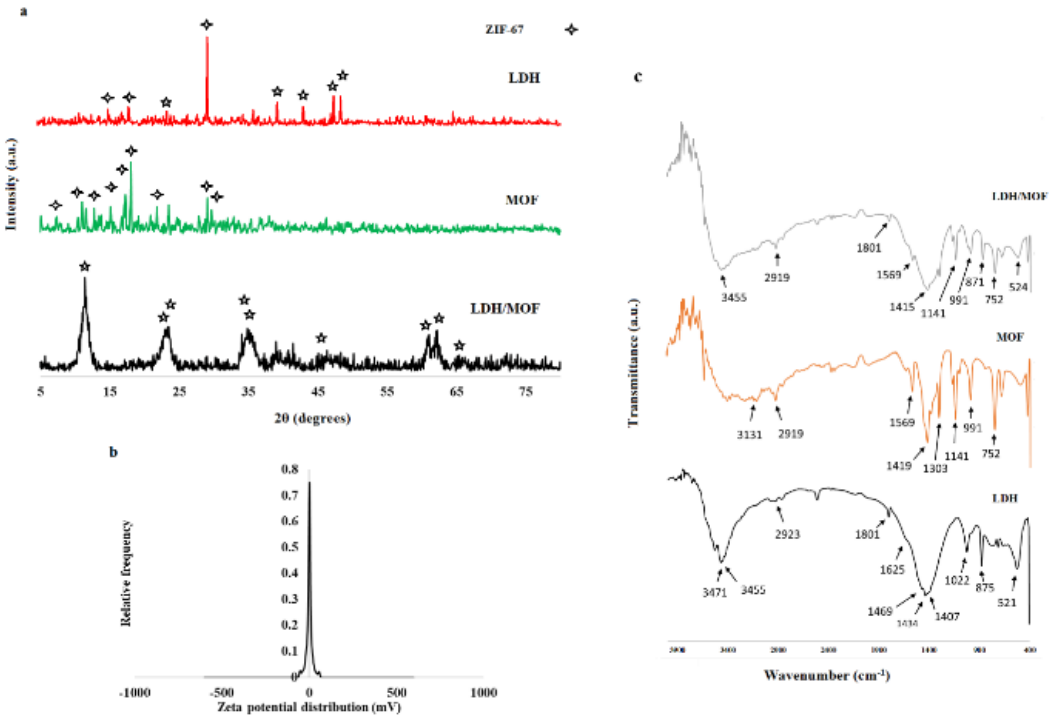

Figure 2. (a) XRD patterns of the synthesized LDH, MOF, and LDH/MOF nanocomposite samples. (b) The zeta potential distribution of LDH/MOF nanocomposite, (c) FTIR spectra of LDH, MOF, and LDH/MOF nanocomposite.

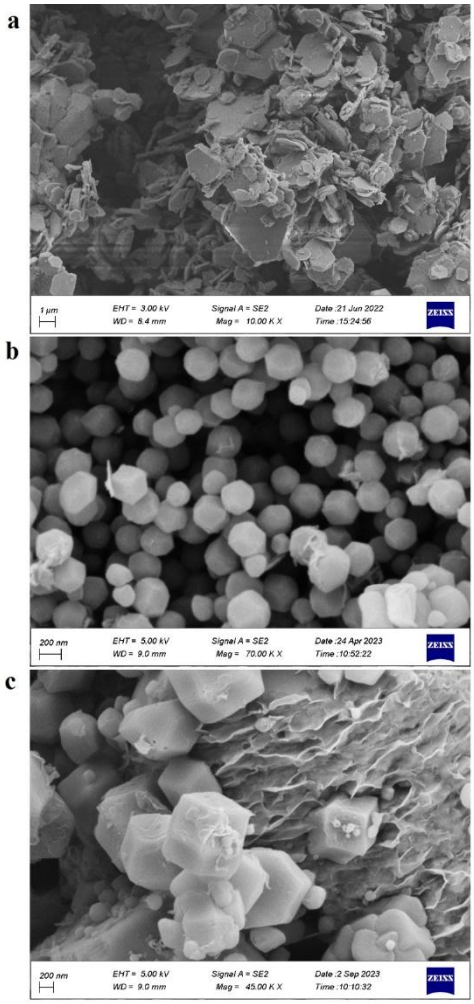

Figure 3. FESEM images of the synthesized (a) LDH nanosheet, (b) MOF, and (c) LDH/MOF nanocomposites.

Figure 4 presents the sorption isotherms and pore size distribution for the LDH, MOF, and LDH/MOF samples. The isotherms of all samples exhibit typical type IV sorption behavior with a hysteresis loop, indicating capillary condensation within mesopores. According to the IUPAC (International Union of Pure and Applied Chemistry) classification, the hysteresis loop can be categorized as H3, suggesting aggregates of plate-like particles that give rise to slit-shaped pores (Malak-Polaczyk et al., 2010). The type IV isotherm with H3 hysteresis primarily originates from the interlayer voids of the LDH structure and the irregular packing of MOF nanoparticles. This hybrid morphology generates additional mesoporous channels at the LDH/MOF interface. The LDH sample has a surface area of 6.53 m^2/g and an average pore diameter of 6.6 nm. The MOF sample exhibits a surface area of 11.2 m^2/g and an average pore diameter of 4.9 nm. The synthesized LDH/MOF nanocomposite shows an enhanced surface area of 60.8 m^2/g, with an average pore diameter of 2.1 nm. These BET results indicate that constructing the Ca–Al LDH and ZIF-67 MOF nanocomposite significantly increases the surface area, which is advantageous for applications such as drug delivery or adsorption.

The synthesized LDH/MOF nanocomposite was evaluated for drug delivery applications through in vitro experiments and compared with the release profiles of LDH and MOF samples. The drug loading efficiency and drug loading capacity of the LDH/MOF sample were determined to be 58% and 19%, respectively. Figure 5a presents the release profile of the drug under acidic and neutral pH conditions. The cumulative amounts of drug released from the LDH sample after 12 h were 56% and 79% under neutral and acidic conditions, respectively. For the MOF sample, the corresponding values were 75% and 81% in neutral and acidic conditions, respectively. The cumulative drug release from the LDH/MOF sample increased to 64% and 85% under pH conditions of 7.4 and 5.5, respectively. The rapid release of the drug from pure ZIF-67 is attributed to its dissolution in water, which facilitates drug liberation. However, when ZIF-67 is shielded by LDH nanosheets, the drug release rate is delayed (Chen et al., 2019). The accelerated release under acidic conditions indicates that this nanocarrier could achieve enhanced drug release in the acidic tumor microenvironment compared to other organs.

The interaction between LDH layers and ZIF-67 nanoparticles primarily occurs through electrostatic attraction, hydrogen bonding between LDH –OH groups and imidazolate linkers, and partial penetration of small ZIF-67 fragments into the expanded LDH interlayers. These combined interactions contribute to the formation of a stable hybrid structure with additional mesoporous channels, consistent with the BET results. Therefore, the synthesized Ca–Al LDH/MOF nanocomposite is a promising candidate for drug delivery applications. The drug loading and release characteristics of the LDH/MOF nanocomposite synthesized in this study are compared with similar works in Table 1. The data in Table 1 highlight that the LDH/MOF sample developed in this research exhibits a higher drug release rate within 12 h under both neutral and acidic conditions.

3.1. Modeling of the drug release kinetic

Several kinetic models are available to describe drug release from dosage forms. Among them, zero-order, first-order, and Korsmeyer–Peppas models are commonly used to characterize in vitro drug release profiles. In the zero-order model, the slow release of the drug from dosage forms that do not disintegrate can be described using Equation (4):

$$Q_t = Q_0 + K_0 t \quad (4)$$

where Q_0 is the initial amount of drug in the solution (usually, $Q_0 = 0$), Q_t is the amount of drug dissolved in time t, and K_0 is the zero-order release constant expressed in units of concentration/time.

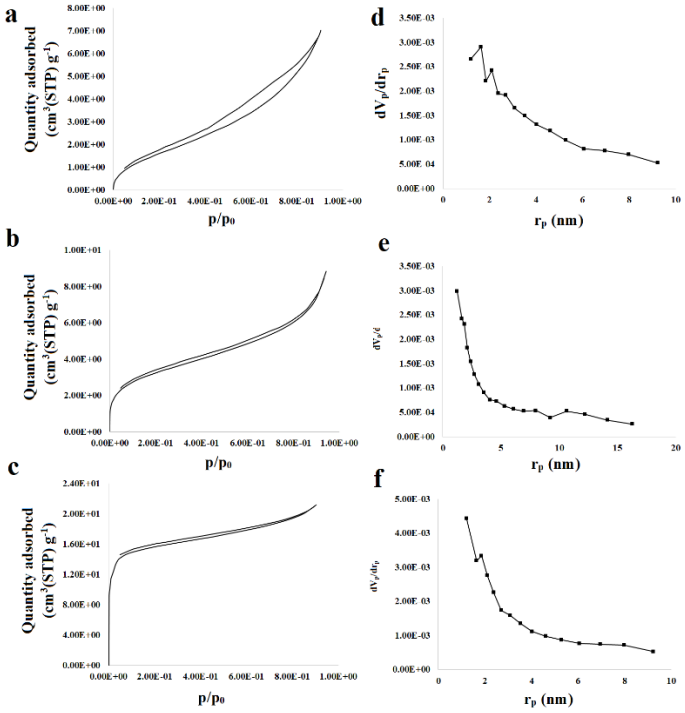

Figure 4. Sorption isotherms for the (a) LDH, (b) MOF, and (c) LDH/MOF samples and corresponding pore size distribution for (d) LDH, (e) MOF, and (f) LDH/MOF samples.

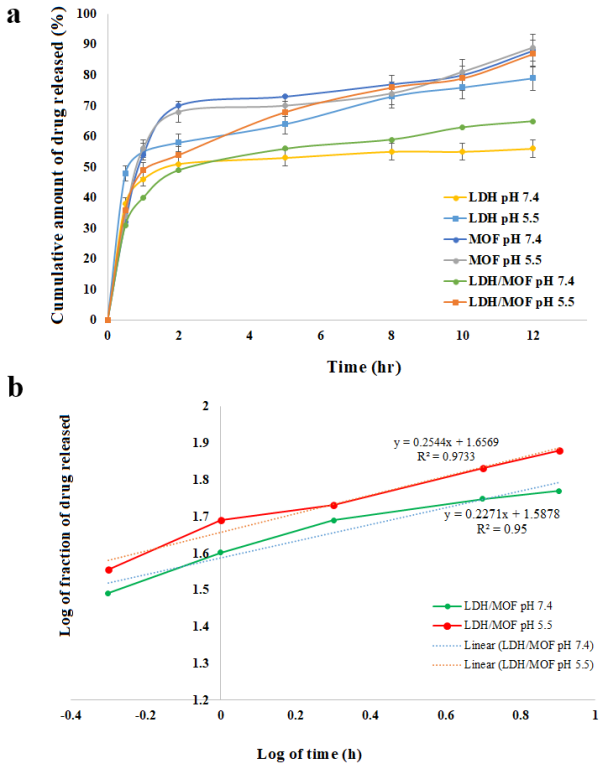

Figure 5. (a) Drug release profile of the LDH, MOF, and LDH/MOF nanocomposite samples in neutral and acidic pH environments; (b) The log of cumulative drug released versus the log of time (h) of the synthesized LDH/MOF nanocomposite which follows the Korsmeyer-Peppas model.

Table 1. The drug loading and release characteristics of the LDH/MOF nanocomposite sample synthesized in current research compared with similar works

LDH/MOF nanocomposite	Model drug	Drug loading/drug encapsulation	Normalized drug release in neutral conditions	Normalized drug release in acidic conditions	Reference
Mg-Al-Ca LDH /Cu MOF-chitosan crosslinked κ-carrageenan hydrogel nanoparticles	DOX	Encapsulation efficiency and drug loading capacity of 96.1 % and 9.6 %, respectively	0.83%/h release	0.31%/h	(Taghikhani et al., 2024)
MgAl-LDH/Fe-MOF	Methotrexate (MTX) and DOX	DOX and MTX loading efficiency and loading capacity of 17.8 %, 3.6 %, 23.2 %, and 4.6 %, respectively	The release rate of 0.21%/h and 0.26%/h in pH 7.4 for MTX and DOX, respectively	The release rate of 0.50%/h and 0.63%/h in pH of 5.0 for MTX and DOX, respectively	(Pooresmaeil & Namazi, 2022)
ZIF-67@Co-LDH yolk-shell heterostructures	Rhodamine 6G	Drug loading capacity of 1.26% and drug loading efficiency of ~78.75%	The concentration of R6G released in water was ~0.54μM/h	-	(Chen et al., 2019)
Ca-Al LDH /ZIF-67	Ciprofloxacin	Drug loading efficiency and drug loading capacity of 58% and 19%, respectively	Drug release of 5.33%/h in pH conditions of 7.4	Drug release of 7.08%/h in pH conditions of 5.5	Current research

In the first-order model, the release of the drug can be described by the following formula:

$$\frac{dC}{dt} = -Kc \quad (5)$$

where K with units of time^{-1} is the first-order rate constant. Equation (4) can be explained as:

$$\log C = \log C_0 - \frac{Kt}{2.303} \quad (6)$$

where K is the first-order rate constant and C_0 is the initial concentration of the drug. It means that in this model, plotting data of the log of cumulative drug percentage versus time results in a straight line with a slope of -K/2.303.

Korsmeyer-Peppas model describes the drug release from polymeric systems and the first 60% of the drug release data is used to check if the release behavior can be explained by this model. This model uses the following formula:

$$\frac{M_t}{M_\infty} = Kt^n \quad (7)$$

where n is the release exponent, k is the release rate constant, and $\frac{M_t}{M_\infty}$ is a fraction of the drug released at time t (Dash et al., 2010). n describes the mechanism of drug release. In the case of cylindrical tablets, n = 1 (0.89) corresponds to case II (zero-order release) transport, n>1 (0.89) is super case II transport (relaxation), 0.5<n<1 corresponds to anomalous (non-Fickian) diffusion, both diffusion, and relaxation, n=0.5 (0.45) is diffusion mechanism, and n<0.5 (0.45) is attributed to quasi-Fickian diffusion (Dash et al., 2010; Sahoo et al., 2012; Siepmann & Peppas, 2012). Through the application of $\frac{M_t}{M_\infty}$<0.6 data, n can be found by plotting the log of cumulative percentage of drug released versus the log of time from the in-vitro drug release data (Dash et al., 2010). Plotting the logarithm of the cumulative drug released from the LDH/MOF nanocomposite against the logarithm of time, as shown in Figure 5b, demonstrates that the drug release profile follows straight lines, with R^2 values of 0.97 and 0.95 for release in environments with pH 5.5 and 7.4, respectively. This indicates that the drug release from the synthesized LDH/MOF nanocomposite in both environments can be described by the Korsmeyer–Peppas model. The release exponent, n, for drug release from the LDH/MOF nanocomposite is 0.25 and 0.22 in environments with pH 5.5 and 7.4, respectively. Therefore, the drug release from the synthesized nanocomposite at both pH values is inferred to occur via quasi-Fickian diffusion (n < 0.5). The low release exponent is likely attributed to the layered structure of LDH, which restricts molecular diffusion, as well as the strong surface adsorption of ciprofloxacin on the MOF active sites.

4. CONCLUSION(S)

The Ca–Al LDH/MOF nanocomposite was synthesized and evaluated as a nanocarrier for drug delivery applications. Phase analysis indicated that the LDH nanosheets have a d-spacing of 4.42 nm, calculated from XRD peak broadening. The in situ synthesis of the

MOF on the LDH nanosheets resulted in an enhanced specific surface area of the nanocomposite. The nanocomposite was successfully loaded with a model drug, ciprofloxacin, achieving a drug loading efficiency and drug loading capacity of 58% and 19%, respectively. Compared with previously reported LDH/MOF systems under similar conditions, the LDH/MOF composite exhibited approximately 35% higher cumulative drug release and a 1.4-fold faster release rate. Drug release in acidic environments was faster than in physiological pH. The release profile of the drug from the synthesized nanocomposite follows the Korsmeyer–Peppas model and is estimated to occur via quasi-Fickian diffusion. Overall, the synthesized nanocomposite shows considerable potential as a nanocarrier for drug delivery applications.

ACKNOWLEDGEMENTS

The author would like to thank the Shahrood University of Technology for the financial support of this project.

REFERENCES

1- Abdallah, B., Elhissi, A. M., Ahmed, W., & Najlah, M. (2020). Carbon nanotubes drug delivery system for cancer treatment. In Advances in Medical and Surgical Engineering (pp. 313-332). https://doi.org/10.1016/B978-0-12-819712-7.00016-4

2- Adegoke, K. A., & Maxakato, N. W. (2021). Porous metal-organic framework (MOF)-based and MOF-derived electrocatalytic materials for energy conversion. Materials Today Energy, 21, 100816. https://doi.org/10.1016/j.mtener.2021.100816

3- Aftab, A., Ahmad, F., Tunio, S. R., Raza, N., Salem, M. E., & Chaudhary, A. A. (2025). A critical review on electrochemical behavior of MOF in supercapacitor. Journal of Organometallic Chemistry, 1042, 123866. https://doi.org/10.1016/j.jorganchem.2025.123866

4- Bai, J., You, Q., Peng, Y., Li, Z., Zhang, Y., Deng, Q., Liao, H., Dong, F., Zeng, X., & Yan, Z. (2025). Utilizing phosphogypsum-derived CaAl LDH-chitosan to remove Pb2+ from oil/gas field wastewater: Adsorption behavior and competitive mechanism. Process Safety and Environmental Protection, 204, 107994. https://doi.org/10.1016/j.psep.2025.107994

5- Barot, J. B., Gupta, S. K., & Gajjar, P. (2025). First-Principles Exploration of the Topological, Optical, and Electronic Transport Behaviors of Novel 2D Ternary Bismuth-Based Compounds. Journal of Physics and Chemistry of Solids, 113291. https://doi.org/10.1016/j.jpcs.2025.113291

6- Behera, N., Duan, J., Jin, W., & Kitagawa, S. (2021). The chemistry and applications of flexible porous coordination polymers. EnergyChem, 3(6), 100067. https://doi.org/10.1016/j.enchem.2021.100067

7- Chen, H., Qian, G., Ruan, X., & Frost, R. L. (2016). Removal process of nickel (II) by using dodecyl sulfate intercalated calcium aluminum layered double hydroxide. Applied Clay Science, 132, 419-424. https://doi.org/10.1016/j.clay.2016.07.008

8- Chen, L., Wang, J., Shen, X., Li, X., & Duan, C. (2019). ZIF-67@ Co-LDH yolk–shell spheres with micro-/meso-porous structures as vehicles for drug delivery. Inorganic Chemistry Frontiers, 6(11), 3140-3145. https://doi.org/10.1039/C9QI00801B

9- Chen, Y.-X., Zhu, R., Xu, Z.-l., Ke, Q.-F., Zhang, C.-Q., & Guo, Y.-P. (2017). Self-assembly of pifithrin-α-loaded layered double hydroxide/chitosan nanohybrid composites as a drug delivery system for bone repair materials. Journal of Materials Chemistry B, 5(12), 2245-2253. https://doi.org/10.1039/C6TB02730J

10- Cosma, M., Mocan, T., Delcea, C., Pop, T., Mosteanu, O., & Mocan, L. (2025). Gold Nanoparticles as Targeted Drug Delivery Systems for Liver Cancer: A Systematic Review of Tumor Targeting Efficiency and Toxicity Profiles. International Journal of Molecular Sciences, 26(16), 7917. https://doi.org/10.3390/ijms26167917

11- Das, S., Roy, S., Dinda, S. C., Bose, A., Mahapatra, C., Basu, B., & Prajapati, B. (2025). Carbon nanotubes in brain targeted drug delivery: A comprehensive review. Results in Chemistry, 102206. https://doi.org/10.1016/j.rechem.2025.102206

12- Dash, S., Murthy, P. N., Nath, L., & Chowdhury, P. (2010). Kinetic modeling on drug release from controlled drug delivery systems. Acta Pol Pharm, 67(3), 217-223. https://www.academia.edu/download/80780512/217.pdf

13- Daud, M., Hai, A., Banat, F., Wazir, M. B., Habib, M., Bharath, G., & Al-Harthi, M. A. (2019). A review on the recent advances, challenges and future aspect of layered double hydroxides (LDH)–Containing hybrids as promising adsorbents for dyes removal. Journal of Molecular Liquids, 288, 110989. https://doi.org/10.1016/j.molliq.2019.110989

14- Deeraj, B. D. S., Jayan, J. S., Raman, A., Asok, A., Paul, R., Saritha, A., & Joseph, K. (2023). A comprehensive review of recent developments in metal-organic framework/polymer composites and their applications. Surfaces and Interfaces, 43, 103574. https://doi.org/10.1016/j.surfin.2023.103574

15- Derbe, T., Temesgen, S., & Bitew, M. (2021). A short review on synthesis, characterization, and applications of zeolites. Advances in Materials Science and Engineering, 2021(1), 6637898. https://doi.org/10.1155/2021/6637898

16- Diop, N. F., Otun, K. O., Thior, S., Maphiri, V. M., Kitenge, V. N., Sarr, S., Sylla, N. F., Wenqiang, X., Chaker, M., Ngom, B. D., & Manyala, N. (2025). Facile room-temperature solution-phase synthesis of a ZIF-67 : Ni hybrid-MOF battery type material for supercapacitor applications. RSC advances, 15(42), 34976-34990. https://doi.org/10.1039/d5ra05741h

17- Elumalai, K., Srinivasan, S., & Shanmugam, A. (2024). Review of the efficacy of nanoparticle-based drug delivery systems for cancer treatment. Biomedical Technology, 5, 109-122. https://doi.org/10.1016/j.bmt.2023.09.001

18- Fattah-alhosseini, A., Karbasi, M., & Bahramian, H. (2023). A thorough investigation of the utilization of metal-organic framework (MOF) coated titanium dioxide in photocatalytic applications: A review. Applied Surface Science Advances, 18, 100504. https://doi.org/10.1016/j.apsadv.2023.100504

19- Figueiredo, M. P., Cunha, V. R., Leroux, F., Taviot-Gueho, C., Nakamae, M. N., Kang, Y. R., Souza, R. B., Martins, A. M. C., Koh, I. H. J., & Constantino, V. R. (2018). Iron-based layered double hydroxide implants: Potential drug delivery carriers with tissue biointegration promotion and blood microcirculation preservation. Acs Omega, 3(12), 18263-18274. https://doi.org/10.1021/acsomega.8b02532

20- Guimarães, D., Cavaco-Paulo, A., & Nogueira, E. (2021). Design of liposomes as drug delivery system for therapeutic applications. International journal of pharmaceutics, 601, 120571. https://doi.org/10.1016/j.ijpharm.2021.120571

21- Ilyes, G. M., Chahinez, B., Saidi-Besbes, S., & Elaissari, A. (2025). Advances in mesoporous silica nanoparticles as carriers for drug delivery and other biomedical applications. Microporous and Mesoporous Materials, 113603. https://doi.org/10.1016/j.micromeso.2025.113603

22- Jadam, M. L., Syed Mohamad, S. A., Zaki, H. M., Jubri, Z., & Sarijo, S. H. (2021). Antibacterial activity and physicochemical characterization of calcium-aluminium-ciprofloxacin-layered double hydroxide. Journal of Drug Delivery Science and Technology, 62, 102314. https://doi.org/10.1016/j.jddst.2020.102314

23- Jiang, N., Wang, Q., Zhang, H., Liu, Z., Yang, H., Chen, R., & Lu, Z. (2023). Low-cost ZIF-67-modified fabrics with effective photothermal disinfection for antimicrobial personal protective equipment production. Journal of Environmental Chemical Engineering, 11(6), 111284. https://doi.org/10.1016/j.jece.2023.111284

24- Jin, C.-X., & Shang, H.-B. (2021). Synthetic methods, properties and controlling roles of synthetic parameters of zeolite imidazole framework-8: A review. Journal of Solid State Chemistry, 297, 122040. https://doi.org/10.1016/j.jssc.2021.122040

25- Jing, C., Dong, B., & Zhang, Y. (2020). Chemical modifications of layered double hydroxides in the supercapacitor. Energy & Environmental Materials, 3(3), 346-379. https://doi.org/10.1002/eem2.12116

26- Karim, A. V., Hassani, A., Eghbali, P., & Nidheesh, P. (2022). Nanostructured modified layered double hydroxides (LDHs)-based catalysts: A review on synthesis, characterization, and applications in water remediation by advanced oxidation processes. Current Opinion in Solid State and Materials Science, 26(1), 100965. https://doi.org/10.1016/j.cossms.2021.100965

27- Karimi, S., Rasuli, H., & Mohammadi, R. (2023). Facile preparation of pH-sensitive biocompatible alginate beads havening layered double hydroxide supported metal-organic framework for controlled release from doxorubicin to breast cancer cells. International Journal of Biological Macromolecules, 234, 123538. https://doi.org/10.1016/j.ijbiomac.2023.123538

28- Kazemi, A., Aghamirza Moghim Aliabadi, H., Afshari, M. H., Tamtaji, M., Baesmat, H., Keshavarz, S., Zeinali, F., Torabi, E., Ferdowsi, G. S., & Manteghi, F. (2025). Porosity Modification in MOF Nanocarriers for pH-Responsive Drug Delivery in Cancer Therapy. ACS Applied Bio Materials, 8(9), 7830-7841. https://doi.org/10.1021/acsabm.5c00838

29- Kitagawa, S., & Matsuda, R. (2007). Chemistry of coordination space of porous coordination polymers. Coordination Chemistry Reviews, 251(21-24), 2490-2509. https://doi.org/10.1016/j.ccr.2007.07.009

30- Kuang, Y., Zhai, J., Xiao, Q., Zhao, S., & Li, C. (2021). Polysaccharide/mesoporous silica nanoparticle-based drug delivery systems: A review. International Journal of Biological Macromolecules, 193, 457-473. https://doi.org/10.1016/j.ijbiomac.2021.10.142

31- Kumari, S., Sharma, V., Soni, S., Sharma, A., Thakur, A., Kumar, S., Dhama, K., Sharma, A. K., & Bhatia, S. K. (2023). Layered double hydroxides and their tailored hybrids/composites: Progressive trends for delivery of natural/synthetic-drug/cosmetic biomolecules. Environmental Research, 238, 117171. https://doi.org/10.1016/j.envres.2023.117171

32- Lawson, H. D., Walton, S. P., & Chan, C. (2021). Metal–organic frameworks for drug delivery: a design perspective. ACS applied materials & interfaces, 13(6), 7004-7020. https://doi.org/10.1021/acsami.1c01089

33- Li, L., Han, J., Huang, X., Qiu, S., Liu, X., Liu, L., Zhao, M., Qu, J., Zou, J., & Zhang, J. (2023). Organic pollutants removal from aqueous solutions using metal-organic frameworks (MOFs) as adsorbents: A review. Journal of Environmental Chemical Engineering, 11(6), 111217. https://doi.org/10.1016/j.jece.2023.111217

34- Mahapatra, D. M., Kumar, A., Kumar, R., Gupta, N. K., Ethiraj, B., & Singh, L. (2025). Artificial intelligence interventions in 2D MXenes-based photocatalytic applications. Coordination Chemistry Reviews, 529, 216460. https://doi.org/10.1016/j.ccr.2025.216460

35- Malak-Polaczyk, A., Vix-Guterl, C., & Frackowiak, E. (2010). Carbon/layered double hydroxide (LDH) composites for supercapacitor application. Energy & fuels, 24(6), 3346-3351. https://doi.org/10.1021/ef901505c

36- Mohamed, A. M., Ramadan, M., & Allam, N. K. (2021). Recent advances on zeolitic imidazolate -67 metal-organic framework-derived electrode materials for electrochemical supercapacitors. Journal of Energy Storage, 34, 102195. https://doi.org/10.1016/j.est.2020.102195

37- Molaei, M. J. (2022). Gadolinium-doped fluorescent carbon quantum dots as MRI contrast agents and fluorescent probes. Scientific Reports, 12(1), 17681. https://doi.org/10.1016/j.optmat.2024.115872

38- Molaei, M. J. (2023a). Carbon quantum dots-based fluorescent layered double hydroxide for targeted drug delivery application. Diamond and Related Materials, 110135. https://doi.org/10.1016/j.diamond.2023.110135

39- Molaei, M. J. (2023b). Magnetic two-dimensional Ca-Al layered double hydroxide/Fe3O4@ dextran nanocomposites as drug delivery systems. Journal of Crystal Growth, 611, 127186. https://doi.org/10.1016/j.jcrysgro.2023.127186

40- Molaei, M. J., & Salimi, E. (2022). Magneto-fluorescent superparamagnetic Fe3O4@ SiO2@ alginate/carbon quantum dots nanohybrid for drug delivery. Materials Chemistry and Physics, 288, 126361. https://doi.org/10.1016/j.matchemphys.2022.126361

41- Möller, K., & Bein, T. (2013). Mesoporosity–a new dimension for zeolites. Chemical Society Reviews, 42(9), 3689-3707. https://doi.org/10.1039/C3CS35488A

42- Nikzamir, M., Hanifehpour, Y., Akbarzadeh, A., & Panahi, Y. (2021). Applications of dendrimers in nanomedicine and drug delivery: A review. Journal of Inorganic and Organometallic Polymers and Materials, 31, 2246-2261. https://doi.org/10.1007/s10904-021-01925-2

43- Patra, C., Guna, V. K., Chakraborty, S., Mondal, S., & Nandakishora, Y. (2025). Advances in 2D Transition Metal Dichalcogenide-Based Gas Sensors. ACS sensors, 10(9), 6347-6379. https://doi.org/10.1021/acssensors.5c02126

44- Plank, J., Dai, Z., & Andres, P. R. (2006). Preparation and characterization of new Ca–Al–polycarboxylate layered double hydroxides. Materials Letters, 60(29), 3614-3617. https://doi.org/10.1016/j.matlet.2006.03.070

45- Pooresmaeil, M., & Namazi, H. (2022). D-mannose functionalized MgAl-LDH/Fe-MOF nanocomposite as a new intelligent nanoplatform for MTX and DOX co-drug delivery. International journal of pharmaceutics, 625, 122112. https://doi.org/10.1016/j.ijpharm.2022.122112

46- Qing, C., Zhang, X.-n., Ding, G.-y., Ma, Y.-f., Zhou, M.-s., & Zhang, Y. (2023). Preparation and biological evaluation of antibody targeted metal-organic framework drug delivery system (TDDS) in Her2 receptor-positive cells. Talanta, 125380. https://doi.org/10.1016/j.talanta.2023.125380

47- Rabiee, N. (2023). Sustainable metal-organic frameworks (MOFs) for drug delivery systems. Materials Today Communications, 35, 106244. https://doi.org/10.1016/j.mtcomm.2023.106244

48- Ramezanzadeh, M., Dashan, A., Norouzi, F., & Ramezanzadeh, B. (2025). Integration of metal co-dopted cysteine builted in porous covalent organic framework (COF) decorated 2D hexagonal boron nitride (h-BN) for multi-functional smart coatings. Journal of colloid and interface science, 680, 311-331. https://doi.org/10.1016/j.jcis.2024.11.063

49- Roondhe, B., Ahuja, R., & Luo, W. (2025). Harnessing the efficiency of twin boron nitride and graphene monolayers for anticancer drug delivery: Insights from DFT. ACS Applied Bio Materials, 8(3), 2015-2026. https://doi.org/10.1021/acsabm.4c01507

50- Roslan, M. Q. J., & Aris, A. Z. (2023). Review: Removal of endocrine-disrupting compounds (EDCs) from water bodies using metal-organic frameworks (MOFs) with diverse linkers incorporating periodic elements and demonstrating high adsorption efficiency. Journal of Environmental Chemical Engineering, 11(6), 111345. https://doi.org/10.1016/j.jece.2023.111345

51- Sahoo, S., Chakraborti, C. K., & Behera, P. K. (2012). Development and evaluation of gastroretentive controlled release polymeric suspensions containing ciprofloxacin and carbopol polymers. J Chem Pharm Res, 4(4), 2268-2284. https://www.researchgate.net/profile/Subhashree-Sahoo-6/publication/375496613

52- Shahabadi, N., Razlansari, M., Zhaleh, H., & Mansouri, K. (2019). Antiproliferative effects of new magnetic pH-responsive drug delivery system composed of Fe3O4, CaAl layered double hydroxide and levodopa on melanoma cancer cells. Materials Science and Engineering: C, 101, 472-486. https://doi.org/10.1016/j.msec.2019.04.004

53- Siepmann, J., & Peppas, N. A. (2012). Modeling of drug release from delivery systems based on hydroxypropyl methylcellulose (HPMC). Advanced Drug Delivery Reviews, 64, 163-174. https://doi.org/10.1016/j.addr.2012.09.028

54- Sun, Z., Park, J.-S., Kim, D., Shin, C.-H., Zhang, W., Wang, R., & Rao, P. (2017). Synthesis and adsorption properties of Ca-Al layered double hydroxides for the removal of aqueous fluoride. Water, Air, & Soil Pollution, 228, 1-7. https://doi.org/10.1007/s11270-016-3160-0

55- Sung, Y. K., & Kim, S. W. (2020). Recent advances in polymeric drug delivery systems. Biomaterials Research, 24(1), 1-12. https://doi.org/10.1186/s40824-020-00190-7

56- Taghikhani, A., Babazadeh, M., Davaran, S., & Ghasemi, E. (2024). Facile preparation of a pH-sensitive biocompatible nanocarrier based on magnetic layered double hydroxides/Cu MOFs-chitosan crosslinked κ-carrageenan for controlled doxorubicin delivery to breast cancer cells. Colloids and Surfaces B: Biointerfaces, 243, 114122. https://doi.org/10.1016/j.colsurfb.2024.114122

57- Thang, N. H., Chien, T. B., & Cuong, D. X. (2023). Polymer-based hydrogels applied in drug delivery: An overview. Gels, 9(7), 523. https://doi.org/10.3390/gels9070523

58- Umdor, R. S., Longchar, I. T., Sharma, S., Umdor, K., & Sinha, D. (2025). LDH composite as an efficient material for the photocatalytic degradation of pharmaceutical pollutants using advanced oxidation process: A review. Journal of Alloys and Compounds, 1022, 179798. https://doi.org/10.1016/j.jallcom.2025.179798

59- Wang, X., Lu, H., Liao, B., Li, G., & Chen, L. (2023). Facile synthesis of layered double hydroxide nanosheets assembled porous structures for efficient drug delivery. RSC advances, 13(18), 12059-12064. https://doi.org/10.1039/D3RA01000G

60- Wang, X., Zhu, J., Zou, F., Zhou, N., Li, Y., & Lei, W. (2022). Ca-Al LDH hybrid self-healing microcapsules for corrosion protection. Chemical Engineering Journal, 447, 137125. https://doi.org/10.1016/j.cej.2022.137125

61- Wekalao, J., Hao, L., Ul Haq, I., & Khan, M. A. (2025). Roadmap to 2D graphene nanomaterials-based biosensors for early cancer detection. Plasmonics, 1-14. https://doi.org/10.1007/s11468-025-02946-0

62- Wu, T., Wu, Z., Shi, Z., Zhang, L., Zhan, Y., Dong, Y., Zhou, B., Wei, F., Zhang, D., & Gao, Y. (2025). Tailoring Interlayer Microenvironment of 2D Layered Double Hydroxides for CO2 Reduction with Enhanced C2+ Production. Small, 21(1), 2406906. https://doi.org/10.1002/smll.202406906

63- Yanar, F., Carugo, D., & Zhang, X. (2023). Hybrid nanoplatforms comprising organic nanocompartments encapsulating inorganic nanoparticles for enhanced drug delivery and bioimaging applications. Molecules, 28(15), 5694. https://doi.org/10.3390/molecules28155694

64- Zhang, P., Qian, G., Shi, H., Ruan, X., Yang, J., & Frost, R. L. (2012). Mechanism of interaction of hydrocalumites (Ca/Al-LDH) with methyl orange and acidic scarlet GR. Journal of colloid and interface science, 365(1), 110-116. https://doi.org/10.1016/j.jcis.2011.08.064